Proceedings of the ASME 2021 Gas Turbine India
GTIndia2021
December 2-3, 2021, Virtual online, India

GTIndia2021-76379

THEORETICAL ESTIMATION OF MINIMUM AND MAXIMUM ALLOWABLE ROTATIONAL SPEED OF SUPERCRITICAL CO_2 INWARD FLOW RADIAL TURBINE

Syed J Hoque[1], Pramod Kumar[1]

[1]Indian Institute of Science, Bengaluru, India

ABSTRACT

Supercritical CO_2 inward flow radial turbines necessitate high operating speeds due to the high density of sCO_2, especially in sub-MW scale power generation where rotational speeds can be in the range of 50k to 150k rpm. Although designing the turbine at these high rotational speeds is reasonable from the aerodynamic efficiency point of view but generally not practical to operate. A theoretical framework based on 1-D meanline analysis is built to evaluate the minimum and maximum rotational speed limits corresponding to a set of boundary conditions and operating constraints. The results show that minimum allowable speed depends on the inlet velocity triangle (IVT) and is constrained by inlet Mach number, inlet blade height, and inlet flow angle. On the other hand, maximum allowable speed depends on the outlet velocity triangle (OVT) and is constrained by outlet relative Mach number, outlet hub radius, and blade speed. The theoretical models are demonstrated from kilowatt to megawatt power levels, and the results are compared with commercial software and Balje's Ns-Ds diagram. Although this study is highlighted in the context of supercritical CO_2 as the working fluid, in principle, the same models are equally valid for any working fluid.

Keywords: sCO_2, specific speed, turbomachine, Ns-Ds diagram, meanline analysis

NOMENCLATURE

sCO_2	Supercritical CO_2
BC	Boundary condition
IVT	Inlet velocity triangle
OVT	Outlet velocity triangle
C	Absolute velocity
U	Blade velocity
W	Relative velocity
ω	Rotational speed
Q	Volumetric flow rate
p	Pressure
T	Temperature
h	Specific enthalpy
s	Specific entropy
Δh	Specific work
a	Sound speed
M	Mach number
ρ	Density
η	Isentropic efficiency
α	Absolute flow angle
β	Relative flow angle
Z_L	Axial length
r	Rotor radius
b	Rotor blade height
ε	Rotor tip clearance
ϕ	Outlet radius ratio
D_s	Specific Diameter
N_s	Specific speed

SUBSCRIPT

0	Stagnation condition
1	Rotor inlet
2	Rotor outlet
h	Hub location
t	Tip location
ts	Total-to-static
m	Meridional direction
r	Radial direction
θ	Tangential direction
W	Relative component
s	Isentropic expansion
min	Theoretical min. limit
max	Theoretical max. limit

SUPERSCRIPT

*	Upper/ Lower bound of operating constraints

1. INTRODUCTION

Supercritical CO_2 (sCO_2) is gaining popularity amongst researchers as the potential working fluid for the next generation thermal power plants. CO_2 has a lower critical temperature of 31.1 °C and critical pressure of 73.8 bar, respectively. CO_2 at its supercritical state exhibits excellent heat transfer properties and chemical stability over a wide range of pressures and temperatures. Presently, sCO_2 technologies are focused on small-scale power generation applications in the field of nuclear power plants [1],[2], concentrated solar power plants [3], and waste heat recovery plants [4]. Inward flow radial turbines are economical for small-scale power generation due to their simple and compact design. The high density of sCO_2 leads to smaller and compact turbine sizes with high rotational speed. Echogen [5] made a size comparison between a 10 MWe conventional steam turbine and a sCO_2 turbine, showing that the sCO_2 turbine is at least five times smaller than the steam turbine. The single-phase operation of sCO_2 leads to low blade erosion even at high temperatures [6]. Also, the low viscosity of sCO_2 reduces losses in turbines. Small size, high rotational speed, and low viscous losses enable the exploration of newer operating regimes and geometries that were unfeasible for air or steam turbines. Hence, there is a need to develop new methodologies, which can design turbomachines at a much lower speed with good efficiencies. This work tries to create a groundwork for the design process by determining the lower and upper limits of rotational speed corresponding to a set of boundary conditions and operating constraints.

2. RADIAL TURBINE OPERATING SPEEDS

The preliminary design of radial turbine requires boundary conditions across the turbine and shaft rotational speed. Stagnation temperature (T_{01}) and stagnation pressure (p_{01}) at the turbine inlet, stagnation or static pressure (p_{02} or p_2) at the outlet, and mass flow rate ($\dot{m}$) are the most used boundary conditions. In this study, subscripts 1 and 2 refer to the rotor inlet and outlet locations, respectively. These boundary conditions are generally obtained from the thermodynamics cycle analysis or heat and mass balance diagram. On the other hand, the rotational speed (ω) of the radial turbine is generally selected using either empirical correlations or from experience.

Balje's specific speed – specific diameter diagram [7] is the most widely used empirical correlation for turbomachinery design. The specific speed (N_s) and specific diameter (D_s) are defined as

$$N_s = \frac{\omega\sqrt{Q_2}}{\Delta h^{3/4}} \quad (1)$$

$$D_s = \frac{2\, r_1\, \Delta h^{1/4}}{\sqrt{Q_2}} \quad (2)$$

where, ω is turbine rotational speed, Q_2 is the volumetric flow rate at the rotor outlet, Δh is specific work and r_1 is rotor inlet radius, all in SI units. Fig. 1 is the Ns-Ds diagram (reproduced in SI units), applicable to the radial turbine, which is a subset of Balje's original Ns-Ds diagram for turbines.

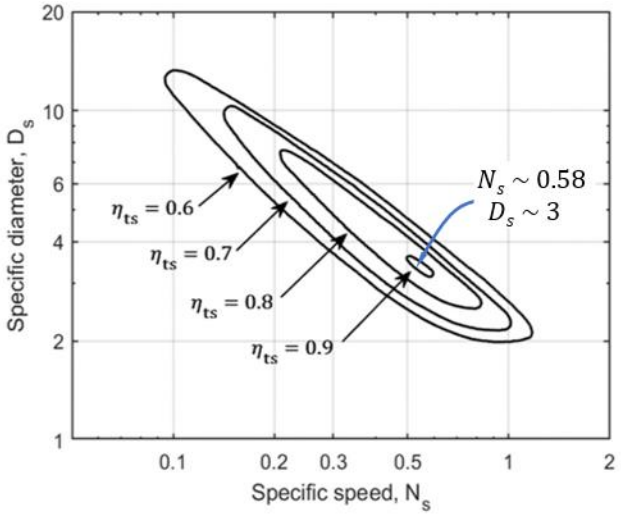

FIGURE 1: BALJE'S Ns-Ds DIAGRAM FOR RADIAL TURBINE

The contours of this diagram represent the experimental results of total-to-static isentropic efficiency (η_{ts}) of radial turbine as a function of specific speed and specific diameter. The diagram shows the maximum efficiency occurs at a specific speed and specific diameter around 0.58 and 3.0, respectively. Hence, all the meanline methodologies available in open literature suggest designing the turbine near this point [8]–[11].

Eq. 1 shows that the high density (or low volumetric flow rate) of sCO_2 necessitates a high rotational speed at the design-point if a specific speed of 0.58 is to be maintained.

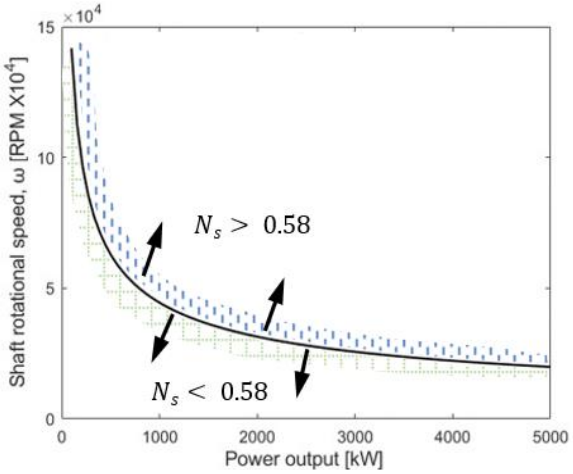

FIGURE 2: VARIATION OF REQUIRED SPEED OF SCO_2 RADIAL TURBINE FOR VARIOUS POWER SCALES CORRESPONDING TO BCs OF TABLE 1, Ns = 0.58, AND Ds =3

Fig. 2 shows the variation of required turbine rotational speed for various power scales (30 kW to 5 MW), while specific speed and specific diameter are maintained at 0.58 and 3.0,

respectively. Table 1 lists the boundary conditions used in Fig. 2. These are typical boundary conditions used for sCO_2 waste heat recovery turbines [12], [13]. Massflow rate is varied according to the scale of power output.

TABLE 1: BOUNDARY CONDITIONS OF A TYPICAL WASTE HEAT RECOVERY sCO_2 TURBINE

Boundary conditions	
Inlet stagnation pressure, p_{01} (bar)	150
Inlet stagnation temperature, T_{01} (°C)	500
Outlet static pressure, p_2 (bar)	100

The figure shows that the required rotational speed increases as the scale of power generation decrease. In the sub-MW scale, the required rotational speed significantly increases from 50k rpm for 1000 kW power output to around 150k rpm for 30 kW power output.

Practically, it is extremely challenging to design a turbine at these high rotational speeds to maintain a specific speed of 0.58. Major limitations could arise from the rotodynamic and material strength to sustain such high rotational speeds. In these cases, a lower operating speed ($N_s < 0.58$) with some loss in efficiency is a more practical choice.

In contrast, there could be instances when the required rotational speed to maintain a specific speed of 0.58 is very low. This could happen for large scale power output or low specific power output. However, sometimes the turbine is forced to operate at a higher speed due to some practical reason. For example, if the turbine is coupled with the compressor, which runs at a higher speed.

One can conclude from the above discussions that depending on the practical situation, the actual rotational speed of the turbine might be lower (low specific speed) or higher (high specific speed) than the recommended one. Referring to Fig. 2, the region below the $N_s = 0.58$ curve represents design-points for low specific speeds and above the curve represents design-points for high specific speeds. As the actual design point differs from the $N_s = 0.58$ curve, the efficiency of the turbine decreases, making a design point too far from the curve unfeasible. A design could be unfeasible due to various reasons such as low efficiency, unacceptable geometry, or some unwanted flow features inside the turbine. These practical restrictions limit the maximum and minimum allowable rotational speed corresponding to a boundary condition beyond which no feasible design exists. These practical limitations are termed 'operating constraints' in this study and are discussed subsequently.

In this study, a MATLAB® [14] based meanline algorithm is developed to find the minimum and maximum rotational speed limits, which is integrated with the REFPROP® [15] fluid database.

3. OPERATING CONSTRAINTS

Fig. 3 shows the 3D model of a radial turbine rotor and its meridional view. Velocity triangles and basic geometrical dimensions as blade height (b), radius (r), and axial length (Z_L), are shown at the mean locations of the inlet (point A) and outlet (point B). Theoretically, a large number of different radial turbines can be designed operating under the same boundary conditions and developing the same power where each design point would give a unique set of rotational speed, velocity triangles, and geometrical dimensions. However, in practice, the flow and geometrical parameters are limited by the 'operating constraints,' limiting the minimum and maximum value of rotational speed.

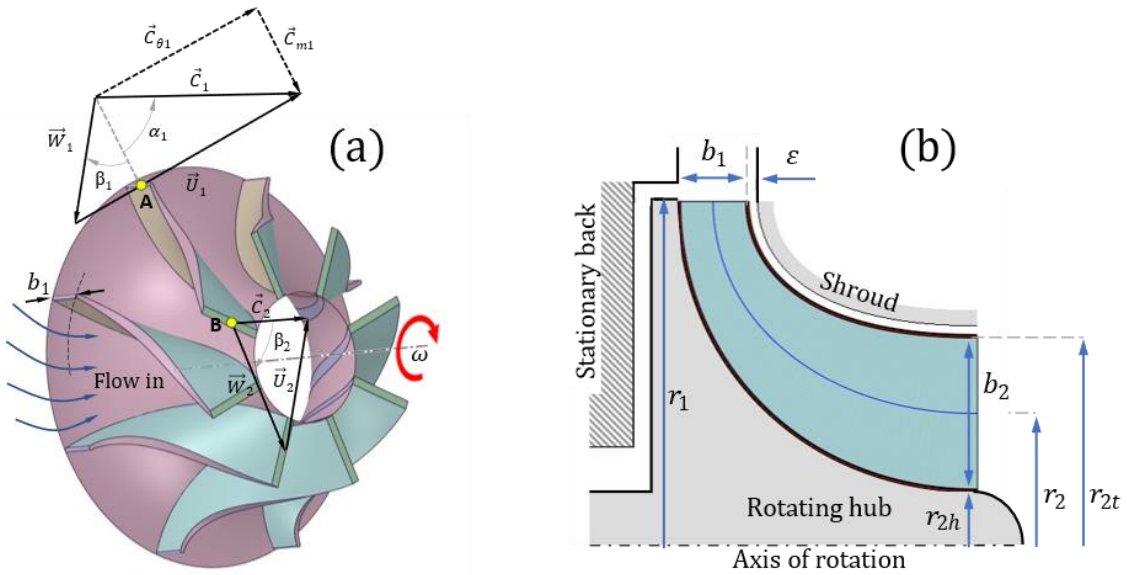

FIGURE 3: GEOMETRIC AND FLOW PARAMETERS OF A RADIAL TURBINE ROTOR (a) 3D MODEL (b) MERIDIONAL VIEW

Here, the term operating constraint combines all the practical restrictions applicable to the radial turbine design, such as geometric size limitations, material strength, manufacturing capability, and flow physics limitations. These constraints range over an upper and lower limit. Table 2 lists various operating constraints used in this study and their boundness discussed below.

TABLE 2: OPERATING CONSTRAINTS, TYPES, AND BOUNDNESS

Operating constraint	Symbol	Constraint Type	Boundness
Blade height	b^*	Geometric	Lower
Mach number	M^*	Flow	Upper
Blade tangential speed	U^*	Material	Upper
Hub (Shaft) radius	r_h^*	Material / Rotodynamic	Lower
Inlet flow angle	α_1^*	Flow	Upper

(i) Blade height: The blade height of the rotor is a geometric constraint, which is bounded by its lower limit. In a radial turbine, blade height at the inlet location (b_1) is the smallest. However, the minimum limit of b_1 is governed by the manufacturing limitations and flow restrictions due to flow passage dimension at inlet. As the inlet blade height decreases, passage becomes narrow, and frictional losses increase because of flow restriction. Also, a small blade height leads to a sizeable relative tip clearance gap (ε/b), causing high leakage losses. So, for all practical purposes, inlet blade height must be above a minimum threshold blade height.

(ii) Mach number: Mach number represents the effect of compressibility, flow losses, and massflow choking. Any turbine operating at high values of Mach number exhibits more losses and flow instabilities that are undesirable for turbine operations. In radial turbines, Mach number associated inlet absolute flow velocity (M_1) and outlet relative flow velocity (M_{w2}) are most important. M_1 represents the losses at the stator outlet and rotor inlet, and M_{w2} represents the losses at the rotor throat and outlet conditions. So, all turbine design procedures, apart from few exceptions, restrict the maximum Mach number below unity.

(iii) Blade tangential speed: The upper bound of blade tangential speed is restricted by the strength of the turbine rotor material. Centrifugal stress is generated by the rotational motion of the rotor, which must be lower than the strength of the rotor material for safe operations. As the centrifugal stress is proportional to the distance from the rotational axis, the inlet radius being the largest in a radial turbine bears the highest stress. In the case of non-radial blading at the inlet (i.e., nonzero metal angle at the inlet), rotational speed leads to bending stresses along the blade height. Therefore, a limit to the maximum allowable value of blade tangential speed is imposed for safer operations.

(iv) Hub radius: The lowest radius of the hub is limited by the shaft radius where the rotor is mounted. The minimum shaft radius is selected based on the material strength and rotodynamic analysis, which is out of the scope of this study. However, it can be appreciated that the shaft radius limits the minimum allowable hub radius.

(v) Inlet flow angle: Referring to the IVT of Fig. 3, inlet absolute flow angle (α_1) decides the ratio of tangential flow to the meridional flow. A high α_1 results in a lower massflow rate through the turbine and ultimately causes lower power output. Standard radial turbine design procedures suggest that the value of α_1 should be less than 80° [11], [16]. Hence, there exists an upper limit of α_1.

There could be more operating restrictions apart from what is discussed above. However, these restrictions are sufficient to develop theoretical models for the minimum and maximum rotational speeds in this study.

4. THEORETICAL MINIMUM ROTATIONAL SPEED

Theoretical minimum rotational speed (ω_{min}) of a turbine represents the lowest possible operating speed corresponding to a set of boundary conditions and operating constraints. Fig. 4 shows various components of the inlet velocity triangle (IVT).

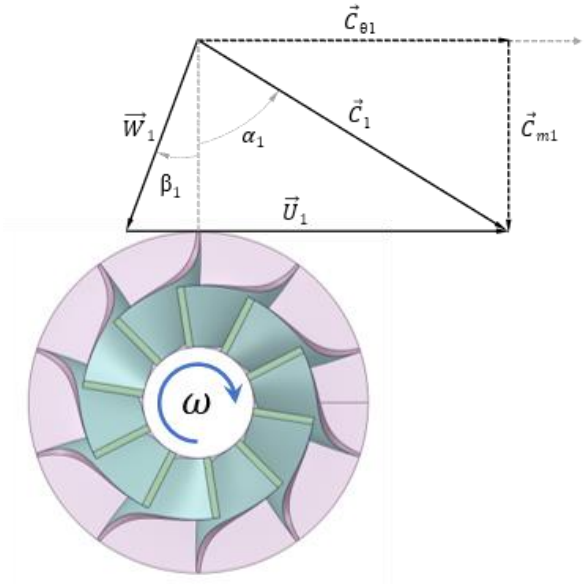

FIGURE 4: INLET VELOCITY TRIANGLE OF RADIAL TURBINE

From thermodynamics, the total-to-static isentropic efficiency of the turbine is defined as

$$\eta_{ts} = \frac{h_{01} - h_{02}}{h_{01} - h_{2s}} = \frac{\Delta h}{\Delta h_s} \tag{3}$$

Euler's equation of turbomachines equates specific work with the change in angular momentum from inlet to outlet as

$$\Delta h = \vec{C}_{\theta 1}\vec{U}_1 - \vec{C}_{\theta 2}\vec{U}_2 \quad (4)$$

In this study, flow at the turbine outlet is assumed to be pure axial ($\vec{C}_{\theta 2} = 0$) which simplifies Eq. 4 as

$$\Delta h = \vec{C}_{\theta 1}\vec{U}_1 \quad (5)$$

From the IVT, the rotational speed is

$$\omega = \frac{U_1}{r_1} \quad (6)$$

and massflow rate at the rotor inlet is

$$\dot{m} = 2\pi r_1 b_1 \rho_1 A_1 C_{m1} \quad (7)$$

where, ρ_1, r_1 and b_1 represents static density, rotor radius, and blade height at the inlet, respectively. Also, the inlet meridional velocity is

$$C_{m1} = C_{\theta 1} \cot \alpha_1 \quad (8)$$

The value of ρ_1 in Eq. 7 depends on the inlet stagnation density (ρ_{01}) and the inlet absolute velocity. The inlet stagnation density depends on known inlet boundary conditions, making the static density a function of absolute velocity.

$$\rho_1 = \rho_1\{C_1\} = \rho_1\{M_1 a_1\} \quad (9)$$

where, M_1 and a_1 are absolute flow Mach number and the speed of sound at the rotor inlet, respectively. Here, the curly bracket expresses the functional relationship of static density with Mach number and speed of sound. Now, combining Eqs. 3 to 9 shows the final form

$$\omega = \frac{2\pi\, \rho_1\{M_1 a_1\}\; b_1\, \Delta h_s\, \eta_{ts}\, \cot \alpha_1}{\dot{m}} \quad (10)$$

Eq. 10 leads to the theoretical minimum speed (ω_{min}) if M_1 and α_1 are at their maximum limits, and b_1 is its minimum limit as per Table 2. The inlet radius of the rotor can be found combining Eqs. 3 to 10 as

$$r_1 = \frac{\dot{m}}{2\pi\, b_1\, \rho_1\{M_1 a_1\} M_1 a_1 \cos(\alpha_1)} \quad (11)$$

Rotor inlet radius corresponding to the ω_{min} denotes the maximum inlet radius ($r_{1\,max}$), which can be found using the same conditions of M_1, α_1 and b_1 used to find ω_{min}. Eqs. 10 and 11 are dependent on the speed of sound at the rotor inlet, which needs to be found iteratively. Fig. 5(a) shows the flow chart of the iterative algorithm used to solve Eqs. 10 and 11.

The above analysis shows that the theoretical minimum speed of a radial turbine depends only on the inlet velocity triangle (IVT). The effect of outlet velocity triangle (OVT) is eliminated by the assumption of pure axial flow at the rotor outlet. In practical cases, radial turbines are designed to have a small negative tangential velocity at the rotor outlet, which helps to recover the exit kinetic energy in the diffuser. So, the actual specific work would become larger than what is presented in Eq. 5, which would slightly increase the ω_{min} of the rotor than what is presented in Eq. 10.

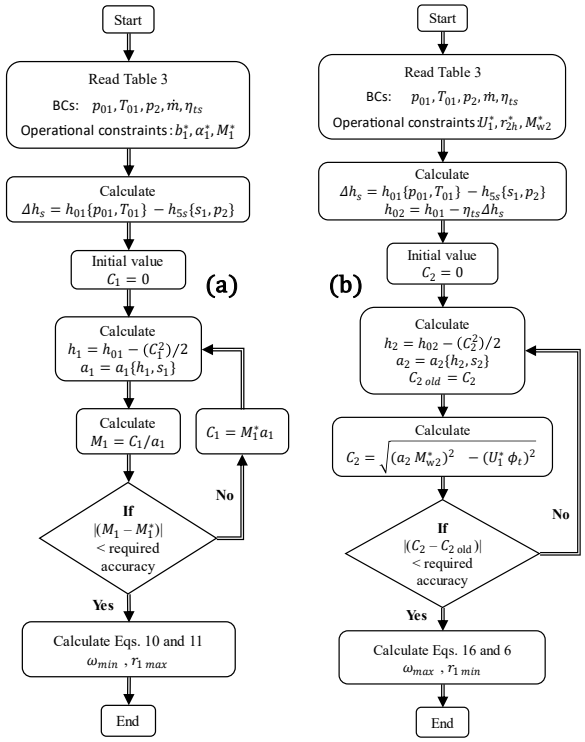

FIGURE 5: COMPUTATIONAL ALGOROTHM OF (a) THEORETICAL MIN. SPEED AND (b) THEORETICAL MAX. SPEED MODELS

5. THEORETICAL MAXIMUM ROTATIONAL SPEED

Theoretical maximum rotational speed (ω_{max}) of a turbine represents the highest allowable operating speed corresponding to a set of boundary conditions and operating constraints.

Eq. 6 shows the rotational speed would be maximum corresponding to a maximum value of U_1 and minimum value of r_1. The maximum value of U_1 is an operating constraint as per Table 2, whereas the minimum value of r_1 depends on both IVT and OVT parameters.

Referring to the meridional view in Fig. 3(b), a lower inlet radius entails increasing the inlet blade height to accommodate the same massflow rate. In the limiting case, inlet blade height would become equal to the inlet radius ($r_{1\,min} \geq b_1$), which puts a restriction to the lower limit to the inlet radius. On the other hand, the lower limit of the inlet radius is also restricted by the minimum outlet area required to accommodate mass outflow.

$$\dot{m} = \pi \rho_2 (r_{2t}^2 - r_{2h}^2) C_2 \quad (12)$$

In practice, r_{2t} must be smaller than r_1, and the minimum value of r_{2h} is an operating constraint, as mentioned in Table 2. Hence, the rotor outlet area decreases with the decrease of r_1. To accommodate the same massflow rate with a lower outlet area, C_2 must increase.

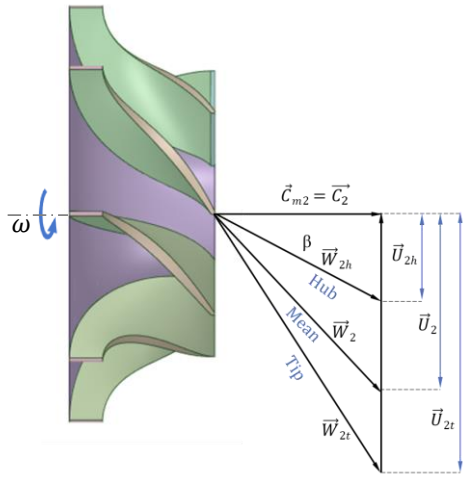

FIGURE 6: DISTRIBUTION OF OVT VELOCITY COMPONENTS ALONG THE OUTLET BLADE HEIGHT

Fig. 6 shows the outlet velocity triangles at the hub, mean, and tip locations assuming pure axial outlet. From the OVT at tip location C_2 is

$$C_2 = \sqrt{(W_{2t}^2 - U_{2t}^2)} \tag{13}$$

Blade speed at the outlet rotor tip is

$$U_{2t} = U_1 \frac{r_{2t}}{r_1} \tag{14}$$

As W_{2t} is the largest velocity component of OVT, Mach number associated with W_{2t} represents the maximum Mach number at the rotor outlet.

$$M_{2w} = \frac{W_{2t}}{a_2} \tag{15}$$

So, the minimum value of the inlet rotor radius ($r_{1\,min}$) is also limited by the maximum value of M_{2w} which is an operating constraint, as mentioned in Table 2.
Now, combining Eqs. 6, 12 – 15, the final form of maximum rotational speed is

$$\omega = U_1 \sqrt{\frac{\pi(\phi_{2t}^2 - \phi_{2h}^2)\sqrt{(a_2^2 M_{2w}^2 - U_1^2 \phi_{2t}^2)}\,\rho_2\{M_2 a_2\}}{\dot{m}}} \tag{16}$$

where, the non-dimensional radius ratio at the outlet hub and tip are

$$\phi_h = \frac{r_{2h}}{r_1} \tag{17}$$

$$\phi_t = \frac{r_{2t}}{r_1} \tag{18}$$

Eq. 16 gives the ω_{max} of the rotor for various radius ratios when U_1, M_{2w} and r_{2h} are at their limits as per Table 2. Notice, the equation is dependent a_2, which cannot be determined in advance, so an iterative approach is required to solve the equation. Fig. 5(b) shows the algorithm used to determine ω_{max} and corresponding radii at the inlet and outlet (Here, outlet radius is algebraic mean of outlet tip and hub radii values).

6. RESULTS

The theoretical models of ω_{min} and ω_{max} are demonstrated using two case studies.

TABLE 3: BCs AND OPERATING CONSTRAINTS FOR CASE STUDIES

Case	1	2
Working fluid	CO_2	CO_2
Power output (kW)	30	5000
Inlet stagnation pressure, p_{01} (bar)	144	205
Inlet stagnation temperature, T_{01} (°C)	220	550
Outlet static pressure, p_2 (bar)	93	95
Massflow rate, $\dot{m}$ (kg/s)	0.9	104
Total-to-static efficiency, η_{ts}	0.8	0.85
Max. inlet flow Mach number, M_1^*	0.6	0.8
Max. outlet relative Mach number, M_{w2}^*	0.6	0.8
Max. inlet absolute flow angle, α_1^*	85°	80°
Min. inlet blade height, b_1^* (mm)	2	10
Min. outlet hub radius, r_{2h}^* (mm)	5	20
Max. blade speed, U_1^* (m/s)	300	400

Table 3 lists the cases and corresponding BCs and operating constraints for which the theoretical models are verified. Power output, boundary conditions, massflow rate, and operating constraints of two cases are selected widely different, which checks the applicability of these proposed theoretical models for a wide range of applications. Results of these models are verified with Axstream®[17], which is industry standard turbomachine modelling commercial software.

6.1 Theoretical min. speed

ω_{min} is obtained by solving Eq. 10 for both the cases, and the results are presented in Fig. 7. Fig. 7(a) and (b) show that

ω_{min} is a function of total-to-static isentropic efficiency and inlet flow Mach number. ω_{min} shows a linear proportional relation with total-to-static isentropic efficiency while showing an inverse relation with inlet flow Mach number.

Fig. 7(c) and (d) present the ω_{min} and corresponding rotor inlet radius for various inlet flow angles and Mach numbers. The figures show a nonlinear relation between ω_{min} and corresponding inlet radius, as per Eq. 11. The design point corresponding to cases 1 and 2, as per Table 3, are also shown using 'star' markers in the figures.

6.2 Theoretical max. speed

ω_{max} is obtained by solving Eq. 16, and the results of both the cases are presented in Fig. 8. Left y-axis represents ω_{max}, and the right y-axis shows inlet and outlet radii. The figure shows that the rotational speed of the turbine initially increases with tip radius ratio, then attains a maximum value and decreases after that. This behavior of ω_{max} can be understood by examining Eq. 16. The tip radius ratio appears twice in the equation; the first one increases the ω_{max} value while the second one decreases it. Hence, the actual variation of ω_{max} depends on the resultant effect of the ϕ_t. Also, the value of ϕ_t corresponding to ω_{max} are different for each case, which is because of different BCs and operating constraints. The figures also show the variation of inlet and mean outlet radii of rotor corresponding to tip radius ratio. Rotor inlet radius attains a minimum at the same tip radius ratio where rotational speed attains the maximum.

These results are compared with the commercial software results in Table 4. The min. operating speeds obtained by the commercial tool are 9-13% higher than the theoretical ω_{min}. The reason could be because the commercial software accounts for losses that are not included in the theoretical model. Also, the outlet flow was not precisely axial in the commercial design because of the hub-to-tip velocity variation.

In contrast, max. operating speeds obtained by the commercial software are 20-25% lower than the theoretical ω_{max} model. The main reason for this high deviation could be because of the considerable exit energy losses due to the high specific speed design [18], apart from the reasons already mentioned for the ω_{min} case. It can be concluded that because of

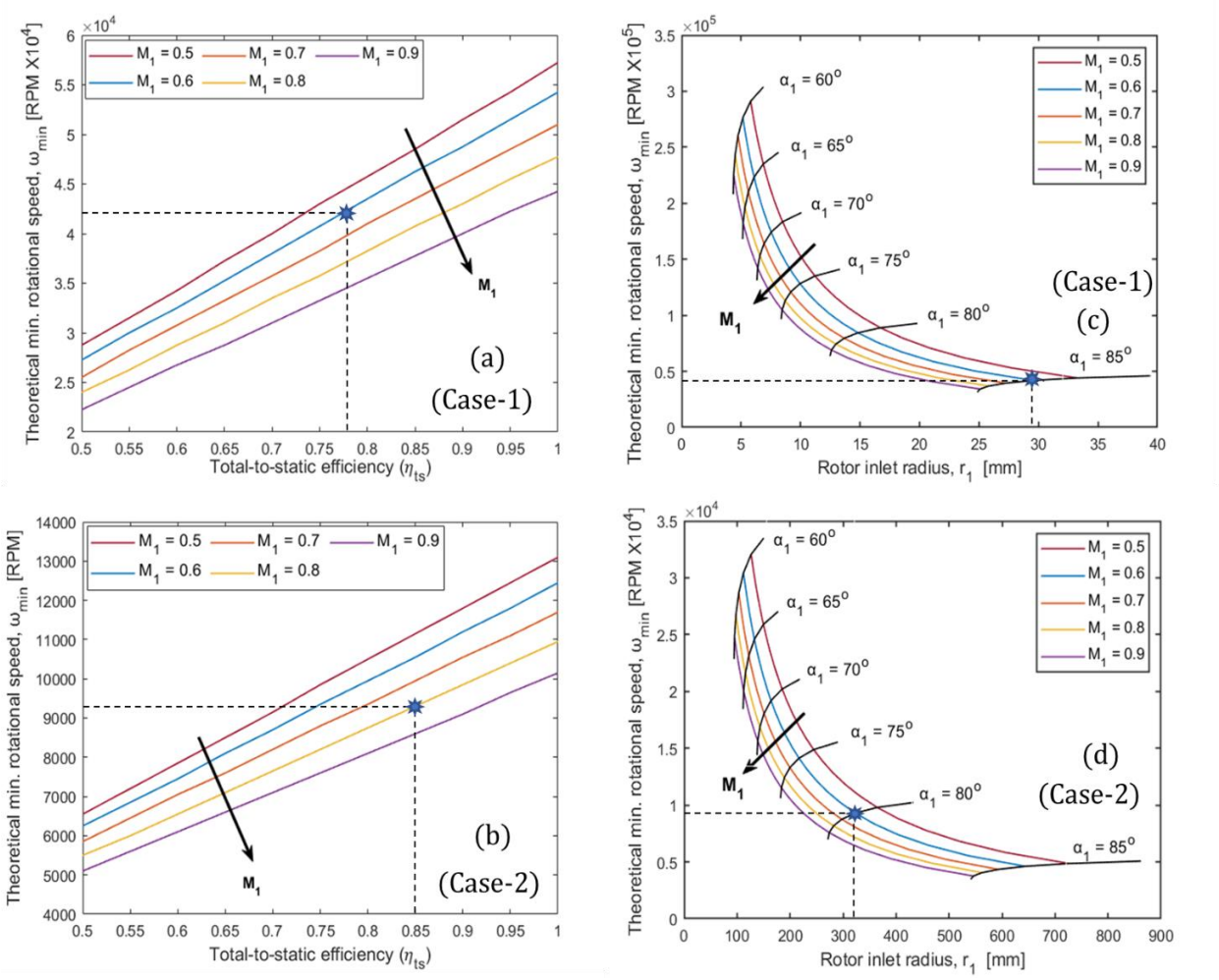

FIGURE 7: EFFECT OF η_{ts}, M_1, AND α_1 ON THE VARIATION OF ω_{min} AND r_{max}

the losses in the turbine, operating speed range shrinks than that of theoretical models.

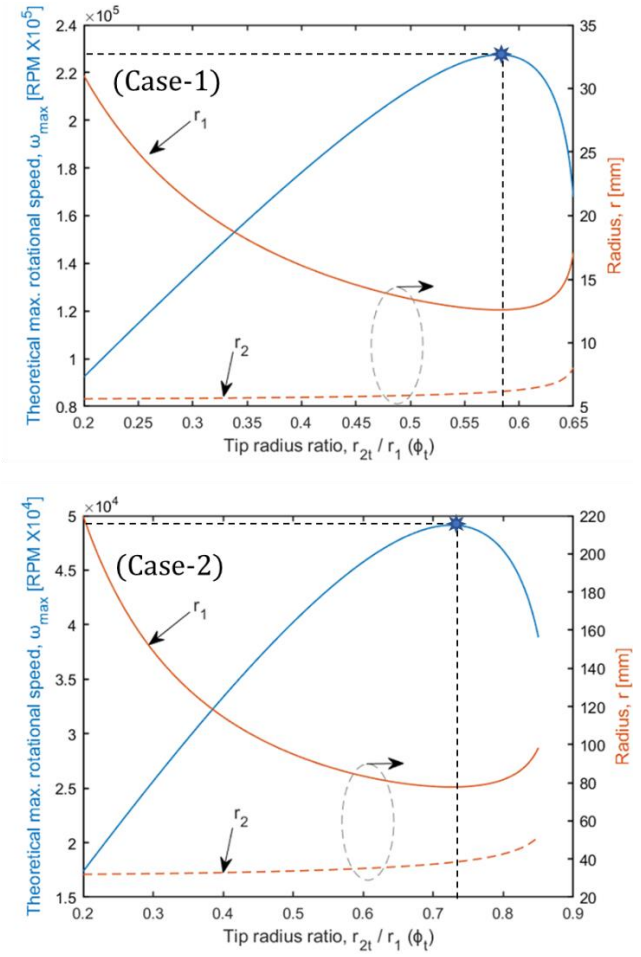

FIGURE 8: VARIATION OF $\boldsymbol{\omega_{max}}$ AND CORRESPONDING $\boldsymbol{r_1}$ AND $\boldsymbol{r_2}$ ALONG VARIOUS $\boldsymbol{\phi_t}$ VALUES

Table 4: RESULT COMPARISON BETWEEN THEORETICAL MODELS AND COMMERCIAL SOFTWARE (Axstream®)

Comparison		Case 1	Case 2
ω_{min} (RPM)	Theoretical model	42,500	9,300
	Commercial software	49,000	10,250
ω_{min} (RPM)	Theoretical model	228,000	49,100
	Commercial software	182,000	40,500

The results obtained from the theoretical models are plotted against Balje's Ns-Ds diagram in Fig. 9. ω_{min} points appear in the top-left corner representing low N_s and high D_s. As ω_{min} corresponds to $r_{1\,max}$, that justifies the low N_s and high D_s values. In contrast, ω_{max} points appear in the bottom-right corner representing high N_s and low D_s as ω_{max} corresponds to $r_{1\,min}$.

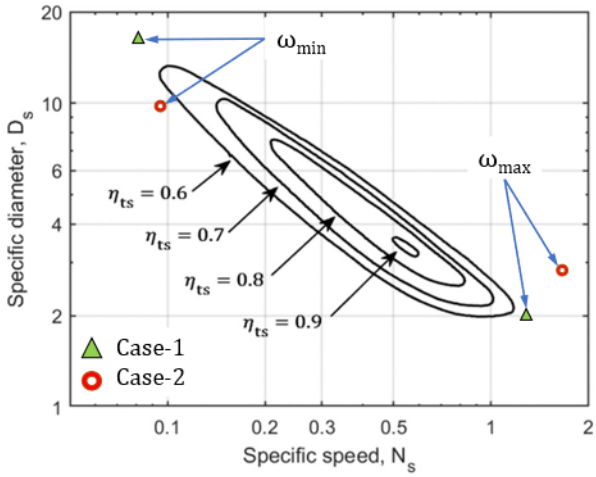

FIGURE 9: COMPARISON OF $\boldsymbol{\omega_{min}}$ AND $\boldsymbol{\omega_{max}}$ MODELS WITH BALJE'S Ns-Ds DIAGRAM FOR TWO CASES

This study was started to find the upper and lower speed limits of Fig. 2. These limits are obtained for the BCs listed in Table 1 and the variation of ω_{min} and ω_{max} are plotted in semi-log scale in Fig. 10. The operating constraints used for this case are $M^* = 0.8$, $\alpha_1^* = 85°$, $b_1^* = 5\ mm$, $U_1^* = 400\ m/s$, $r_h^* = 10\ mm$.

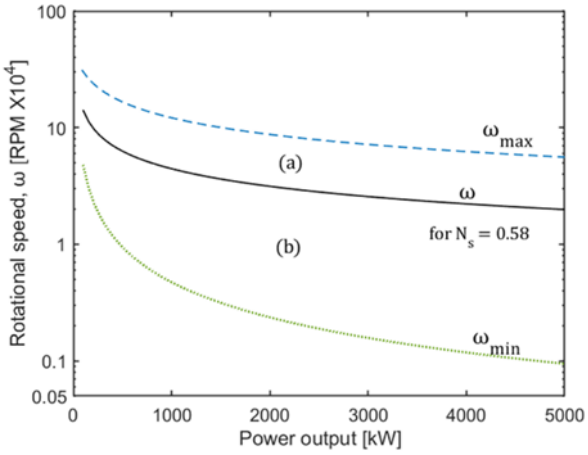

FIGURE 10: VARIATION OF $\boldsymbol{\omega_{min}}$ AND $\boldsymbol{\omega_{max}}$ FOR DIFFERENT POWER SCALES CORRESPONDING TO BCs IN TABLE 1

In this figure, region (a) represents the high specific speed design area, and region (b) represents the low specific speed region. The region between the ω_{min} and ω_{max} curves represent the possible speed regime where a turbine can be designed, and outside this area turbines cannot be designed.

7. CONCLUSION

The study presents theoretical 1D models to find the maximum and minimum speed limits of a radial turbine without going for the actual design process. The models show ω_{min} and ω_{max} are solely dependent on the boundary conditions and operating constraints. Both the models can predict speed limits from kilowatt to megawatt scale turbines with reasonable accuracy. The ω_{min} model shows a difference of 9-13%, whereas ω_{max} model shows a higher difference of 20-25% compared to the commercial software. The main reason for this deviation is the losses inside the turbine, which shrinks the operating speed limits. These models also show good agreement with Balje's Ns-Ds chart. As the models are developed from the fundamental laws of turbomachines, the same models hold true irrespective of the working fluid.

ACKNOWLEDGEMENTS

The authors acknowledge Department of Science and Technology, Government of India for financial support vide sanction order(s): TMD/CERI/CSP/2020/1(G) dated 21-09-2020, and TMD/CERI/Clean Coal/2017/034 (IISc) (G) dated 13-09-2018. The inputs from Triveni Turbines Limited and Tata Consulting Engineers (TCE), Bangalore in carrying out this work is also gratefully acknowledged.

REFERENCES

[1] A. Moisseytsev and J. J. Sienicki, "Investigation of alternative layouts for the supercritical carbon dioxide Brayton cycle for a sodium-cooled fast reactor," *Nucl. Eng. Des.*, 2009, doi: 10.1016/j.nucengdes.2009.03.017.

[2] Y. Ahn and J. I. Lee, "Study of various Brayton cycle designs for small modular sodium-cooled fast reactor," *Nucl. Eng. Des.*, 2014, doi: 10.1016/j.nucengdes.2014.05.032.

[3] T. Neises and C. Turchi, "A comparison of supercritical carbon dioxide power cycle configurations with an emphasis on CSP applications," 2014, doi: 10.1016/j.egypro.2014.03.128.

[4] O. H. Us, "Supercritical carbon dioxide power cycle for waste heat recovery," vol. 2, no. 12, 2013, [Online]. Available: https://patents.google.com/patent/US9341084B2/en.

[5] M. Persichilli, A. Kacludis, E. Zdankiewicz, and T. Held, "Supercritical CO 2 Power Cycle Developments and Commercialization: Why sCO 2 can Displace Steam Ste am," *Power-Gen India Cent. Asia*, pp. 1–15, 2012, [Online]. Available: http://www.echogen.com/documents/why-sco2-can-displace-steam.pdf.

[6] H. J. Lee, H. Kim, and C. Jang, "Compatibility of Candidate Structural Materials in High-Temperature S-CO2 Environment," *4th Int. Symp. - Supercrit. CO2 Power Cycles*, pp. 1–9, 2014.

[7] O. E. Baljé, "A study on design criteria and matching of turbomachines: Part A-similarity relations and design criteria of turbines," *J. Eng. Gas Turbines Power*, vol. 84, no. 1, 1962, doi: 10.1115/1.3673386.

[8] D. Japikse, "Introduction to turbomachinery analysis.," 1984.

[9] A. Whitfield, "The preliminary design of radial inflow turbines," *Proc. ASME Turbo Expo*, vol. 1, no. January 1990, 1989, doi: 10.1115/89GT83.

[10] A. J. Glassman, "Enhanced analysis and users manual for radial-inflow turbine conceptual design code RTD," *NASA Contract. Rep. 195454*, no. Lewis Research Center, 1995.

[11] R. H. Aungier, *Turbine Aerodynamics: Axial-Flow and Radial-Flow Turbine Design and Analysis*. 2010.

[12] G. Manente and F. M. Fortuna, "Supercritical CO2 power cycles for waste heat recovery: A systematic comparison between traditional and novel layouts with dual expansion," *Energy Convers. Manag.*, vol. 197, no. April, p. 111777, 2019, doi: 10.1016/j.enconman.2019.111777.

[13] S. J. Hoque and · Pramod Kumar, "Analysis of a Dual Recuperated Dual Expansion Supercritical CO 2 Cycle for Waste Heat Recovery Applications," *Trans. Indian Natl. Acad. Eng.*, vol. 6, pp. 439–459, 2021, doi: 10.1007/s41403-021-00211-4.

[14] MATLAB, *version 7.10.0 (R2020a)*. Natick, Massachusetts: The MathWorks Inc., 2020.

[15] E. W. Lemmon, M. L. Huber, M. O. McLinden, and others, "NIST standard reference database 23."

[16] S. Dixon and C. Hall, *Fluid Mechanics and Thermodynamics of Turbomachinery*. 2010.

[17] "Axstream_Product-Brochure_August_2017.pdf." .

[18] H. Rohlik, "Analytical determination of radial inflow turbine design geometry for maximum efficiency.," *NASA TN D-4384.1969.*, 1969.